SCIENCE CHINA
Physics, Mechanics & Astronomy

Temperature-dependent evolution of surface charge screening and polarization at ferroelectric surfaces

LongFei Wang, Yi Luo, JieSu Wang, XiuShi Huang, ZhaoMeng Gao, TieYing Yang, XiaoLong Li, Pei Li, KuiJuan Jin, WeiFeng Zhang and HaiZhong Guo

Citation: SCIENCE CHINA Physics, Mechanics & Astronomy **62**, 987721 (2019); doi: 10.1007/s11433-018-9301-2

View online: http://engine.scichina.com/doi/10.1007/s11433-018-9301-2

View Table of Contents: http://engine.scichina.com/publisher/scp/journal/SCPMA/62/8

Published by the Science China Press

SCIENCE CHINA
Physics, Mechanics & Astronomy

•Letter to the Editor•

August 2019 Vol. 62 No. 8: 987721
https://doi.org/10.1007/s11433-018-9301-2

Temperature-dependent evolution of surface charge screening and polarization at ferroelectric surfaces

LongFei Wang[1], Yi Luo[2], JieSu Wang[3], XiuShi Huang[1], ZhaoMeng Gao[1], TieYing Yang[4], XiaoLong Li[4], Pei Li[1], KuiJuan Jin[3], WeiFeng Zhang[1*], and HaiZhong Guo[1,2*]

[1] *Henan Key Laboratory of Photovoltaic Materials, School of Physics and Electronics, Henan University, Kaifeng 475004, China;*
[2] *School of Physical Engineering, Zhengzhou University, Zhengzhou 450001, China;*
[3] *Beijing National Laboratory for Condensed Matter Physics, Institute of Physics, Chinese Academy of Sciences, Beijing 100190, China;*
[4] *Shanghai Synchrotron Radiation Facility (SSRF), Shanghai Institute of Applied Physics, Chinese Academy of Sciences, Shanghai 201204, China*

Received June 22, 2018; accepted September 11, 2018; published online February 25, 2019

Citation: L. F. Wang, Y. Luo, J. S. Wang, X. S. Huang, Z. M. Gao, T. Y. Yang, X. L. Li, P. Li, K. J. Jin, W. F. Zhang, and H. Z. Guo, Temperature-dependent evolution of surface charge screening and polarization at ferroelectric surfaces, Sci. China-Phys. Mech. Astron. **62**, 987721 (2019), https://doi.org/10.1007/s11433-018-9301-2

The polarization and domain behavior on the surface of a ferroelectric material are significantly affected by the screening processes [1-12]. Recently, there has been a notable increase in the theoretical calculations and experiments investigating the dynamics of polarization and domain behaviors coexisting in phase transitions of ferroelectric materials. There is thus a widespread interest in the dynamics of the screening charges on ferroelectric surfaces [8-14]. On the other hand, $BaTiO_3$ (BTO), has attracted the attention as it can be used for memory-related devices, multilayer capacitors, electro-optic devices, and for other applications, because of its ferroelectricity, excellent electro-optic, and nonlinear optical properties [9,15-17]. The structure of BTO changes from a tetragonal ferroelectric phase to a cubic paraelectric one at the Curie temperature of 120°C [18-20]. There has been a remarkable interest on the investigation of the dynamics of surface screening and the temperature dependence of polarization of the ferroelectric surfaces. For example, Kalinin et al. [9-11] investigated the domain polarity and temperature-induced potential inversion on a BTO (100) surface. Yuan et al. [18] reported the evolution of ferroelectric domains from 20 to 120°C for a BTO film. Gu et al. [5,6] evaluated the dynamics of surface screening charges on ferroelectric $BiFeO_3$ films. Chen et al. [21] investigated the surface potential of the poled domains formed by applying different voltages at a $Pb(Zr_xTi_{1-x})O_3$ film. Even though the effects of the surface screening on the ferroelectric thin films have been investigated by changing the temperature or the applied voltage, a more detailed and systematic investigation of the evolution of the surface potential decay process and polarization with varying temperature is still rare.

In this work, the temperature-dependent evolutions of the polarization reversal, surface potential, and surface potential decay process were investigated by a combination of scanning probe microscopy techniques, high-resolution synchrotron X-ray diffractometry (SXRD) and the second-harmonic generation (SHG) method. Scanning probe microscopy techniques with a commercial experiment instrument (Asylum Research MFP-3D Infinity) comprised atomic force microscopy (AFM), piezoresponse force microscopy (PFM), and surface Kelvin probe force microscopy (KPFM) were performed. Our findings provide a pathway to improve the BTO film performance at the optimal temperature;

*Corresponding authors (WeiFeng Zhang, email: wfzhang@163.com; HaiZhong Guo, email: hguo@zzu.edu.cn)

moreover, the stability could be enhanced particularly for data storage applications.

The BTO thin films were grown via pulsed laser deposition on (001) STO substrates with a 12-nm-thick $La_{0.5}Ca_{0.5}MnO_3$ (LCMO) buffered layer as the bottom electrode. A detailed description of the process is included in the Supporting Information. The structure and crystalline qualities of the LCMO layer and BTO/LCMO/STO heterostructure were identified using SXRD, shown in Figure S1(a) and (b), respectively. The results indicate that the LCMO and BTO layers are both high-quality single-phases. The surface topography images of LCMO layer and BTO layer was evaluated by AFM, shown in Figure S1(c) and (d). They both exhibit a smooth and dense surface.

The relationship between temperature and phase transition was investigated for the BTO thin film. For this, the temperature-dependent SXRD 2θ-θ scans were obtained around the (002) diffraction peaks of BTO, LCMO, and STO from 20 to 400°C. The experiments were performed using the high-resolution SXRD at the BL14B1 beam line of the Shanghai Synchrotron Radiation Facility (SSRF), with 1.24 Å X-rays and Huber 5021 six-axis diffractometry, shown in Figure S2. This trend is clearly observed when plotting the lattice constants, obtained from the 2θ-θ scan curves, as a function of temperature, Figure 1. The increase of the LCMO and STO lattice constants is linear and is due to the thermal expansion. However, the BTO thin film behavior shows an anomaly at around 120°C, and the (002) peak of BTO is split into two peaks when the temperature reaches this value, indicating the coexistence of two phases. This coexistence is possible because of the gradual relaxation of phase transition. Also, it is worth noting that the phase transition temperature of bulk BTO is approximately 120°C. However, because of the influence of the buffer layer, the transition temperature of BTO near the buffered layer may change. The lattice constants corresponding to these two peaks are shown in Figure 1.

The optical SHG method is a powerful tool to explore the symmetry of noncentrosymmetric structures [22]. As shown in Figure 2(a) and (b), a reflective SHG optical path was used to measure SHG data and thus explore the temperature-dependent structural properties. P-OUT in Figure 2(a) corresponds to the analyzer polarization parallel to the plane of incidence, considering a rotating polarization of the incident light; S-OUT in Figure 2(b) is the analyzer polarization perpendicular to the plane of incidence. To further evaluate the SHG changes, the SHG intensities were obtained from P-OUT at 0°, and S-OUT at 45°, where the intensity is respectively the maximum for each curve. The SHG intensities at different temperatures are shown in Figure 2(c), where the maximum intensity is observed at around 120°C. As a simple example of nonlinear optic processes, the optical SHG response is a frequency-doubled light wave emitted by the

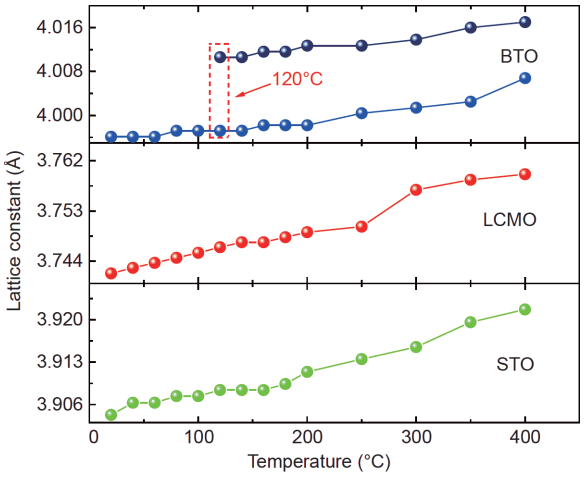

Figure 1 (Color online) Lattice constants of BTO, LCMO, and STO at different temperatures.

polarization (P) in a material, induced by the fundamental incident light wave, whose intensity can be usually expressed as $I(2\omega) \propto |P(2\omega)|^2$ [22]. It can be seen from Figure 2(c) that the SHG intensities of both the P-OUT and S-OUT signals increase with temperature, reaching a maximum at around 140°C, and then decrease. Therefore, the most sensible structural response of the BTO film on SHG may be at 140°C. The temperature-dependent SHG behavior is consistent with the SXRD results, which indicate that a structural phase transition occurs at temperatures over 120°C. This also indicates that SHG is more sensitive to the structural information than the surface polarization of the ferroelectric thin film.

As seen in Figure S3(a), the BTO film is flat and uniform. The evolution of the out-of-plane phase (OP) PFM images with temperature is shown in Figures S3(b)-(f). The OP-PFM measurements of the BTO thin film at different temperatures show the most stable polarization reversal and enhanced ferroelectric properties at 60-80°C. Figure S4 shows the piezoresponse phase-voltage hysteresis and the butterfly-like amplitude-voltage loops obtained for the BTO/LCMO/STO heterostructure when varying the temperature. These results indicate that the piezoelectric response improves at 80°C.

KPFM has been widely utilized to evaluate the surface charge state (or surface potential) of materials. It is a pure surface probing technique that directly measures the difference in potential between the tip and the sample. The obtained value includes variations in the work function of the materials, and the effect of trapped charges and of any applied bias. Figure 3(a) shows the schematic representation of the local poling process of ferroelectric films using a conductive AFM tip. At room temperature (about 20°C), the KPFM color contrast is not very clear, shown in Figure 3(b). However, as temperature increases (Figure 3(c) and (d)), the contrast becomes clearer, being most notable at 80°C. It has been reported that the sideways diffusion of the surface

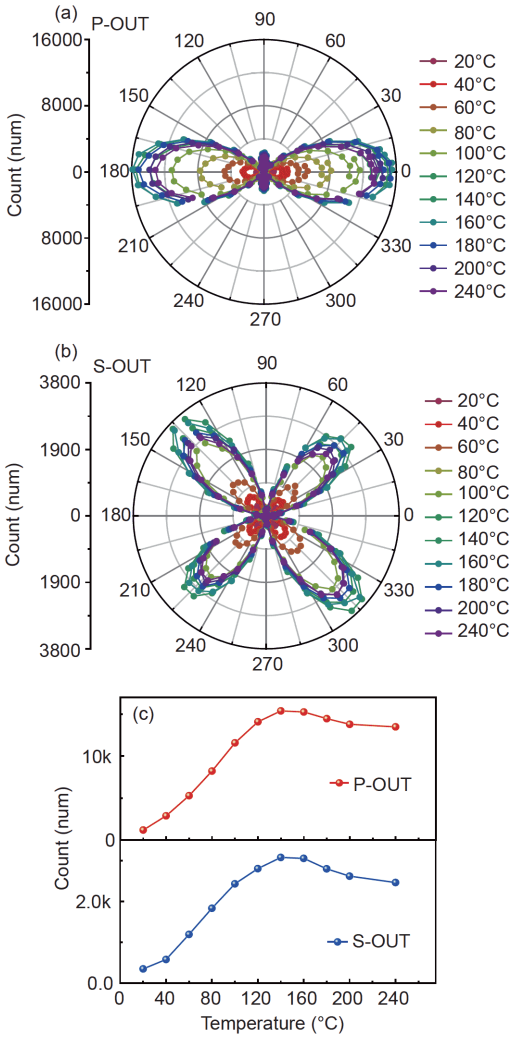

Figure 2 (Color online) SHG anisotropy patterns at different temperatures under (a) perpendicular and (b) parallel configurations. The colored circles are experimental data, and are linked to explicitly show the shapes of the SHG curves (c).

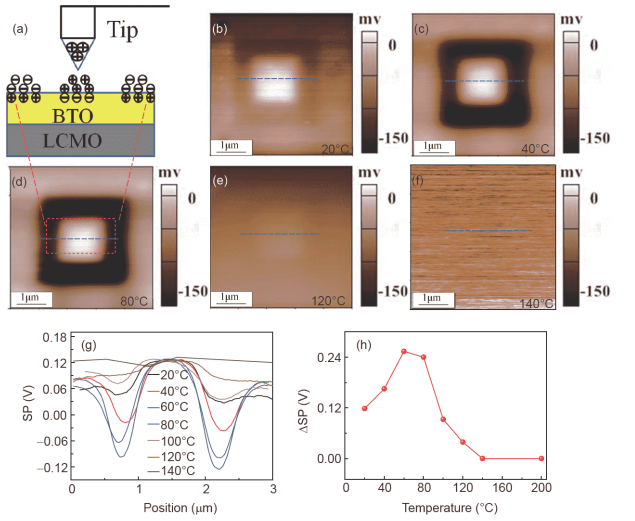

Figure 3 (Color online) (a) Scheme representing the local poling process of the ferroelectric film with a conductive AFM tip. Overscreened charges are accumulated on the surface of the sample during the bias-induced domain switching. The KPFM images of the 5 μm×5 μm area in the BTO/LCMO/STO heterostructure at (b) 20°C, (c) 40°C, (d) 80°C, (e) 120°C, and (f) 140°C during the heating process; the ±5 V polarized regions are marked with dashed black squares. (g) Line profile of the KPFM image (green lines) in the (b)-(f) KPFM images, the colors (A-F-H) represent different temperatures (20°C-120°C-20°C). (h) ΔSP as a function of temperature.

charges dominates the evolution of the screening charge decay process [22]. Therefore, the unclear KPFM image at room temperature may be due to the unstable polarization and the surface charge rapidly spreading toward both sides. Then, as the temperature increases, the polarization reversal stabilizes, reaching the maximum stabilization at 80°C. The surface charge diffusion speed decreases, thus the contrast becomes clear. This also agrees with the temperature-dependent PFM measurements (Figure S2). Finally, as the temperature continues to rise (Figure 3(e) and (f)), the contrast begins to fade again and nearly disappears at 140°C. This is due to the proximity to the ferroelectric-paraelectric phase transition (120°C) of BTO. When the BTO structure changes from tetragonal to cubic phase, the ferroelectricity begins to decrease and the overscreened charges are gradually released when approaching 120°C. Figures S5(a)-(d) show the KPFM images of BTO at 60 and 100°C during heating and cooling, as it can be seen, there are no notable changes between the two images for each temperature.

The temperature-dependent evolution of the surface potential (SP) is displayed in Figure 3(g). The plots correspond to profile of the KPFM image marked by the green dashed lines in Figure 3(b)-(f). The high and low SP correspond to the tip-injected positive and negative overscreened surface charges on the downward- and upward-polarized domains, respectively. ΔSP was extracted from the KPFM potential images at different temperatures after poling, shown in Figure 3(h). The data from the heating and cooling processes are respectively represented by red and black dots. The ΔSP values in the heating process are 0.24, 0.32, 0.50, 0.48, 0.18, 0.06 and 0 V for 20, 40, 60, 80, 100, 120, and 140°C, respectively.

As clearly observed in Figure 3(g) and (h), the ΔSP value is the largest at 60-80°C. This can be explained by two mechanisms. First, the temperature dependence of the potential is attributed to the complete screening of polarization bound charges, resulting in the formation of an electric double layer [9]. This may also be valid for the BTO surface. Accordingly, increasing the temperature results in the sensitive piezoelectric response, promoting the incomplete screening of the charges. Thus the gradual accumulation of the bound charge produces an electric dipole layer in the BTO film, yielding a sufficiently large coercive field that increases the effective surface potential. Furthermore, the charges accumulate and the screening charges reache a dynamic equilibrium between 60-80°C. The corresponding ΔSP value is thus the highest, shown in the Figure 3(h).

When the temperature of the BTO film is over 80°C, the transition from the ferroelectric to the paraelectric phase occurs, and the domain stepwise transformation weakens the piezoelectric response. Polarization gradually disappears, and the effect of the piezoelectric response on the bound charges is minimal, then the decrease in the intensity of the bound charges immediately causes the ΔSP to become smaller. Second, the surface screened charge stability changes at different temperatures. The tip-injected charges likely begin to diffuse sideways once the tip contacts the surface with an applied bias. Due to technological limitations, it is not possible to polarize a region while simultaneously detecting the SP distribution. Therefore, the ΔSP values vary with temperature. To assess this, the ΔSP evolution was plotted at different temperatures, Figure 4.

Figure S7(a)-(e) show the KPFM potential diagram at different temperatures. At 20, 40, 60, 80, and 100°C, the initial values of ΔSP are 0.44, 0.51, 0.58, 0.56, and 0.46 V, then the values decrease with time. The evolution of ΔSP and normalized-ΔSP are plotted in Figure 4(a) and (b). It can be clearly seen in Figure 4(b) that the screened charges on the surface decay with time at the different temperatures, at 20, 40, 60, 80, and 100°C the ΔSP reach to 41%, 68%, 77%, 74%, and 55% of their initial values. Therefore, it can be concluded that the decrease of the overscreened charges on BTO is the slowest at 60 and 80°C, further confirming that the ferroelectric properties are more stable and stronger at this temperature range.

In conclusion, the dynamics of the surface charge screening and polarization at the ferroelectric surface of a BTO thin film were investigated. With increasing temperature, the piezoelectric response and coercive voltage of the BTO film notably increase at 60°C and 80°C. The decay of the ΔSP value at different temperatures in the polarization region is the slowest at 60–80°C. The temperature-dependent results show a stable polarization reversal, very slow screening electric decay, and the enhancement of the ferroelectric performance and surface charge states of the BTO surface at this temperature range. This investigation could contribute to improving the BTO film performance by temperature control, and could also help with the data stability in charge storage. This is crucial to the stabilization of ferroelectric domains, data storage density, and non-volatile bit readout.

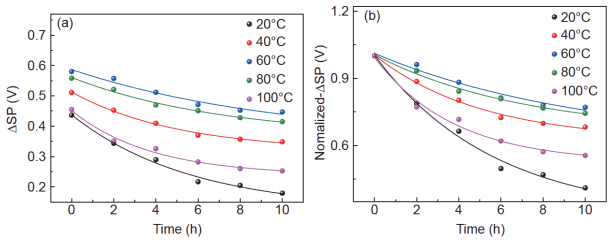

Figure 4 (Color online) The time-evolution of the (a) ΔSP and (b) normalized-ΔSP images of the BTO film at 20, 40, 60, 80°C, respectively.

This work was supported by the National Natural Science Foundation of China (Grant No. 11574365). The authors thank beam line BL14B1 (Shanghai Synchrotron Radiation Facility) for providing the beam time and helps during experiments.

Supporting Information

The supporting information is available online at phys.scichina.com and http://link.springer.com/journal/11433. The supporting materials are published as submitted, without typesetting or editing. The responsibility for scientific accuracy and content remains entirely with the authors.

1 G. B. Stephenson, and M. J. Highland, Phys. Rev. B **84**, 064107 (2011), arXiv: 1101.0298.
2 Y. Jang, Y. D. Park, J. A. Lim, H. S. Lee, W. H. Lee, and K. Cho, Appl. Phys. Lett. **89**, 183501 (2006).
3 X. D. Liu, H. X. Baoyin, and X. R. Ma, Sci. China-Phys. Mech. Astron. **56**, 818 (2013).
4 S. Tong, W. I. Park, Y. Y. Choi, L. Stan, S. Hong, and A. Roelofs, Phys. Rev. Appl. **3**, 014003 (2015).
5 J. Gu, K. Jin, C. Ge, C. Ma, and G. Yang, AIP Adv. **6**, 015220 (2016).
6 J. Gu, K. Jin, L. Wang, X. He, H. Guo, C. Wang, M. He, and G. Yang, J. Appl. Phys. **118**, 204103 (2015).
7 V. Likodimos, X. K. Orlik, L. Pardi, M. Labardi, and M. Allegrini, J. Appl. Phys. **87**, 443 (2000).
8 J. Wang, K. Jin, H. Yao, J. Gu, X. Xu, C. Ge, C. Wang, M. He, and G. Yang, Appl. Phys. Lett. **112**, 102904 (2018).
9 S. V. Kalinin, and D. A. Bonnell, Appl. Phys. Lett. **78**, 1116 (2001).
10 S. V. Kalinin, C. Y. Johnson, and D. A. Bonnell, J. Appl. Phys. **91**, 3816 (2002).
11 S. V. Kalinin, and D. A. Bonnell, Nano Lett. **4**, 555 (2004).
12 Y. Kim, M. Park, S. Bühlmann, S. Hong, Y. K. Kim, H. Ko, J. Kim, and K. No, J. Appl. Phys. **107**, 054103 (2010).
13 Y. L. Li, S. Choudhury, J. H. Haeni, M. D. Biegalski, A. Vasudevarao, A. Sharan, H. Z. Ma, J. Levy, V. Gopalan, S. Trolier-McKinstry, D. G. Schlom, Q. X. Jia, and L. Q. Chen, Phys. Rev. B **73**, 184112 (2006).
14 Z. Gao, X. Huang, P. Li, L. Wang, L. Wei, W. Zhang, and H. Guo, Adv. Mater. Interfaces **5**, 1701565 (2018).
15 Q. Wan, K. J. Jin, Q. Q. Li, Y. Q. Feng, C. Wang, C. Ge, M. He, H. B. Lu, H. Z. Guo, X. L. Li, Y. P. Yang, and G. Z. Yang, Sci. China-Phys. Mech. Astron. **60**, 057711 (2017).
16 Y. Feng, C. Wang, S. L. Tian, Y. Zhou, C. Ge, H. Z. Guo, M. He, K. J. Jin, and G. Z. Yang, Sci. China-Phys. Mech. Astron. **60**, 067711 (2017).
17 H. Guo, Q. Li, Z. Yang, K. J. Jin, C. Ge, L. Gu, X. He, X. Li, R. Zhao, Q. Wan, J. Wang, M. He, C. Wang, H. Lu, Y. Yang, and G. Yang, Sci. Rep. **7**, 7693 (2017).
18 G. Yuan, J. Chen, H. Xia, J. Liu, J. Yin, and Z. Liu, Appl. Phys. Lett. **103**, 062903 (2013).
19 R. Tazaki, D. Fu, M. Itoh, M. Daimon, and S. Y. Koshihara, J. Phys.-Condens. Matter **21**, 215903 (2009).
20 H. Guo, L. Liu, Z. Chen, S. Ding, H. Lu, K. Jin, Y. Zhou, and B. Cheng, Europhys. Lett. **73**, 110 (2006).
21 X. Q. Chen, H. Yamada, T. Horiuchi, K. Matsushige, S. Watanabe, M. Kawai, and P. S. Weiss, J. Vac. Sci. Technol. B **17**, 1930 (1999).
22 J. S. Wang, K. J. Jin, H. Z. Guo, J. X. Gu, Q. Wan, X. He, X. L. Li, X. L. Xu, and G. Z. Yang, Sci. Rep. **6**, 38268 (2016).